Direct fabrication of Cu/Cu_2O composite micro-temperature sensor using femtosecond laser reduction patterning

Mizue Mizoshiri[1]*, Yasuaki Ito[1], Shun Arakane[1], Junpei Sakurai[1], and Seiichi Hata[1]

[1] *Department of Micro-Nano Systems Engineering, Graduate School of Engineering, Nagoya University, Nagoya 464-8603, Japan*

E-mail: mizoshiri@mech.nagoya-u.ac.jp

Micro-temperature sensors, which composed of a Cu_2O-rich sensing part and two Cu-rich electrodes, were directly fabricated by femtosecond laser reduction patterning of CuO nanoparticles. Patterning of the microstructures was performed by laser scanning with pitches of 5, 10, and 15 μm. Cu_2O-rich micropatterns were formed at the laser scan speed of 1 mm/s, the pitch of 5 μm, and the pulse energy of 0.54 nJ. Cu-rich micropatterns that had high generation selectivity of Cu against Cu_2O were fabricated at the laser scan speed of 15 mm/s, the pitch of 5 μm, and the pulse energy of 0.45 nJ. Electrical resistivities of the Cu_2O-rich and Cu-rich micropatterns were approximately 10 Ωm and 9 μΩm, respectively. The temperature coefficient of the resistance of the micro-temperature sensor fabricated under these laser irradiation conditions was -5.5×10^{-3}/°C. This resistance property with a negative value was consistent with that of semiconductor Cu_2O.

1. Introduction

Laser direct-writing technology has received attention in recent years because it can be applied to three-dimensional printing and additive manufacturing of metal structures. For example, selective laser sintering (SLS) was used for the fabrication of 3D structures[1-4]. 2D layered structures are interconnected to form 3D structures by sintering raw metal powders. If we try to apply this process to fabricate 3D metal microstructures, the raw metal powders must be downsized. However, the downsized metal powders are easily oxidized in their preparation and setting processes. Moreover, SLS must be conducted under a vacuum condition to prevent reoxidation of the 3D metal microstructures.

Printed electronics technology is also one of the direct-writing technologies developed for the fabrication of 2D metal micropatterns[5-11]. Metal micropatterns were formed using metal nanoparticle ink with subsequent sintering for metallization. To improve the laser energy absorption of the raw nanoparticles (NPs), laser reductive sintering using metal oxide NPs has been reported[12-16]. In these processes, metal oxide NPs such as CuO or NiO NPs were reduced, agglomerated, and sintered to form metal micropatterns. For example, CuO NP solution was prepared by mixing CuO NPs, poly(vinyl pyrrolidone) (PVP), and ethylene glycol (EG) as a reducing agent[12]. Cu micropatterns were formed using continuous-wave (CW) and nanosecond laser-induced reduction of the CuO NPs in air. NiO NPs were reduced to form Ni micropatterns using toluene as a reducing agent[15-16]. To date, we also fabricated Cu micropatterns using femtosecond laser reduction patterning of CuO NPs. Recently, Cu_2O-rich and Cu-rich micropatterns were selectively fabricated by optimizing the reductive temperature controlled by femtosecond laser irradiation conditions[17]. Furthermore, the generated Cu_2O-rich and Cu-rich micropatterns revealed semiconductor-like negative and metal-like positive temperature coefficients of resistance, respectively[18]. If we could fabricate Cu_2O-rich and Cu-rich microstructures selectively by simply controlling the laser irradiation conditions of the CuO NP solution, highly sensitive micro-sensors, composed of metal oxide sensing parts and metal electrodes, could be formed in a single-step process using femtosecond laser direct patterning.

For example, the use of Cu_2O thin films has been reported in gas, humidity, and temperature sensors[19-25]. Metal oxide materials with large absolute temperature coefficients of resistance performed efficiently in the detection of gas, humidity, and temperature as a

large resistance difference. In general, these sensors were fabricated using well-established microfabrication processes such as lithography and vacuum deposition. Our direct selective fabricating metal oxide and metal micropatterns in the air is effective for fabricating microdevices with composite materials.

In this study, we fabricated a micro-temperature sensor composed of a Cu_2O-rich sensing part and Cu-rich electrodes, using femtosecond laser reduction patterning of CuO NPs. First, we evaluated the optimal raster scan pitch to form micropatterns. Then, we evaluated the electrical resistivity of the Cu_2O-rich and Cu-rich micropatterns. Finally, the whole micro-temperature sensor was directly fabricated by femtosecond laser reduction patterning under optimal laser irradiation conditions.

2. Experimental methods

2.1 Design and fabrication of the micro-temperature sensor

Figure 1(a) shows the design of a micro-temperature sensor. The sensing part and their electrodes were formed using Cu_2O-rich and Cu-rich micropatterns. The size of the sensing part was 100 × 200 μm^2, including the connecting the area to the electrodes. The gap between the electrodes was 100 μm. The Cu_2O-rich and Cu-rich micropatterns were selectively formed by femtosecond laser reduction patterning of CuO NPs. Figure 1(b) shows a schematic illustration of the fabrication process. First, CuO NP solution was spin-coated on a glass substrate. Then, the Cu-rich electrodes were formed by raster scanning of the focused femtosecond laser pulses. The Cu_2O-rich sensing part was subsequently formed. These laser irradiations were performed in air. Finally, the non irradiated CuO NPs were removed by rinsing in EG and ethanol. The exposure dose for patterning was controlled by the laser irradiation conditions such as the laser scan speed, the raster scan pitch, and the pulse energy.

2.2 Material preparation

CuO NP solutions were prepared by mixing CuO NPs (<50 nm particle size, Sigma Aldrich), EG (99.8%, Sigma Aldrich), and PVP (M_w≈10000, Sigma Aldrich) using ultrasonic waves. The concentration of CuO NPs, EG, and PVP were 60, 27, and 13 wt%, respectively[12, 16]. The CuO NP solution was spin-coated onto a glass substrate (approximately 1.3 mm thick) at the spinning rate of 7000 rpm. The film thickness of the CuO NP solution was 8 μm.

2.3 Femtosecond laser scanning system

We used a femtosecond fiber laser (Toptica Photonics, FemtoFiber pro.) in the laser scanning system. The pulse duration, wavelength, and repetition rate of the laser were 120 fs, 780 nm, and 80 MHz, respectively. The femtosecond laser pulses were focused onto the CuO NP solution film on the glass substrate using an objective lens with a numerical aperture of 0.80. Patterning of the microstructures was performed by scanning the sample substrate using an XYZ mechanical stage and a mechanical shutter. The pulse energy of the laser was 0.17−0.54 nJ.

2.4 Evaluation of the micropatterns and the micro-temperature sensor

Crystal structures of the micropatterns were evaluated using an X-ray micro-diffractometer (Rigaku RINT RAPID-S) equipped with a Cu-Kα radiation source. The X-ray was collimated to 0.3 mm in diameter. The microstructures for the evaluation were 2×1 mm^2, which was large enough to irradiate the X-ray with the incident angle of 20°.

Electrical resistivity of the micropatterns was examined using a four-terminal system (Mitsubishi Chemical Analytech, Loresta GP). The microstructures were formed on a glass substrate with the size of 1×5 mm^2.

The resistance of the micro-temperature sensor was measured under various temperatures controlled using a hot plate in air. Before the measurement, Cu_2O-rich micropatterns of the sensing part was overcoated with SiO_2 thin films (thickness: 100 nm) by radio-frequency (RF) magnetron sputtering to prevent reoxidation. The resistance was measured using an electronic multimeter.

3. Results and discussion

3.1 X-ray diffraction spectra of the micropatterns

Figures 2(a) and 2(b) show an optical microscope image and a scanning electron microscopy (SEM) image of the line pattern fabricated by laser irradiation, respectively. The scanning speed and the pulse energy of the laser were 20 mm/s and 0.17 nJ, respectively, which was the minimum exposure dose in our experiment. Figures 2(c) and 2(d) show the line patterns in optical microscope and SEM images, respectively, obtained the conditions that the scan

speed was 1 mm/s and the pulse energy was 0.54 nJ, which was the maximum exposure dose in our experiment. Both optical microscope images showed that the metallic luster was almost the same in the melted areas in the respective SEM images. The minimum line width of the pattern was approximately 5–10 μm at the scan speed of 20 mm/s and the pulse energy of 0.17 nJ.

By taking account of the width of the line patterns, we fabricated the micropatterns by laser raster scanning of focused laser pulses with pitch larger than 5 μm. The electrically connected micropatterns are expected under these conditions. Figure 3 shows one of the X-ray diffraction (XRD) spectra of the micropatterns. The laser scan speeds were 1, 5, 10, 15, and 20 mm/s, and the pulse energy was 0.54 nJ. All the micropatterns contained Cu, Cu_2O, and CuO.

To evaluate the degree of the reduction of CuO NPs to generate Cu and Cu_2O, we compared the intensity ratios of the XRD spectra. The intensity of the $Cu_2O(111)$ peak divided by that of the CuO(111) peak was expressed as $I_{Cu2O(111)}/I_{CuO(111)}$. The intensity of the Cu(111) peak divided by that of the $Cu_2O(111)$ peak was expressed as $I_{Cu(111)}/I_{Cu2O(111)}$, which exhibits the generation selectivity of Cu against Cu_2O. This value is useful for fabricating Cu-rich electrodes that exhibit the lower effect of semiconductor-like Cu_2O. Figures 4(a)-4(c) show the relationship between the intensity ratio of $I_{Cu2O(111)}/I_{CuO(111)}$ at the raster scan pitches of 5, 10, and 15 μm, respectively. Little Cu_2O was generated at the pitch of 15 μm, because the exposure dose was too low to reduce the raw CuO NPs. The maximum value of $I_{Cu2O(111)}/I_{CuO(111)}$ was obtained at the laser scan speed of 1 mm/s, the raster scan pitch of 5 μm, and the pulse energy of 0.54 nJ. The Cu_2O-rich micro-temperature sensing part was fabricated at the scan speed of 1 mm/s, the raster scan pitch of 5 μm, and the pulse energy of 0.54 nJ. Figures 4(d)-4(f) show the relationship between the intensity ratio of $I_{Cu(111)}/I_{Cu2O(111)}$ at the raster scan pitches of 5, 10, and 15 μm, respectively. The value of $I_{Cu(111)}/I_{Cu2O(111)}$ was maximum at the scan speed of 10 mm/s, the scan pitch of 15 μm, and the pulse energy of 0.54 nJ, as shown in Figs. 4(d)-4(f). However, in comparison with the values of $I_{Cu2O(111)}/I_{CuO(111)}$ at the pitches of 5 and 10 μm, the values at the pitch of 15 μm were extremely smaller (0.1–1.4), as shown in the inset of Fig. 4(c). To reduce the resistance of the electrodes and the temperature dependence of the resistance by increasing the generation selectivity of Cu against Cu_2O, Cu-rich electrodes were formed at the scan speed

of 15 mm/s, the raster scan pitch of 5 μm, and the pulse energy of 0.45 nJ, where the maximum value of $I_{Cu(111)}/I_{Cu2O(111)}$ was obtained with the exception of the condition that the scan pitch was 15 μm. The generation degrees of Cu_2O and Cu were considered to be determined by the valance of the reduction of CuO NPs and reoxidation of Cu in the micropatterns[18]. In comparison of the total irradiation energy for the fabrication of Cu_2O-rich and Cu-rich micropatterns, the Cu_2O-rich micropatterns were formed at a higher total energy than that in the case of Cu-rich micropatterns. When the scan pitch was 5 μm, the generation degree of Cu_2O increased with decreasing scan speed under a higher pulse energy condition (0.45 and 0.54 nJ), as shown in Fig. 4(a). Under a lower pulse energy condition (0.28 and 0.17 nJ), Cu_2O increased upon decreasing the scan speed in the range of 10-20 mm/s. On the other hand, Cu_2O decreased at the scan speed of 5 mm/s, but then increased again at the scan speed of 1 mm/s when the scan speed was decreased. These results suggest that Cu_2O was generated by the reduction of CuO NPs in the range of 10-20 mm/s, and Cu_2O was generated by the reoxidation of the reduced Cu at 1 mm/s. The condition that the scan speed was 5 mm/s possibly caused the effects of maximal reduction and minimum reoxidation. Therefore, the Cu_2O-rich micropatterns, which were fabricated under the higher total energy condition, the scan speed of 1 mm/s, the raster scan pitch of 5 μm, and the pulse energy of 0.54 nJ, were considered to be generated by the reoxidation of the reduced Cu in the micropatterns.

Electrical resistivities of the Cu_2O-rich and Cu-rich micropatterns were approximately 10 Ωm and 9 μΩm, respectively. The thickness of the films were assumed to be 8 μm, which was the thickness of the as-coated CuO NP solution film because no significant total volume change upon removing CuO NPs was observed in the laser-irradiated area during the removal of non-laser irradiated CuO NPs, even though the deformation of the surface occurred. These values are approximately 10^6 times and 10^3 times larger than those of the bulk Cu_2O (1–10 μΩm) and Cu materials (16.8 nΩm), respectively[26-30]. The high electrical resistivity was induced by the lower density of the structures and contamination such as residual carbon. However, the temperature coefficient of resistance of the carbon was not dominant for those of the Cu_2O-rich and the Cu-rich micropatterns because the XRD peaks associated with carbon were not observed, as shown in Fig. 3.

3.2 Fabrication and evaluation of the micro-temperature sensor

Optical microscope and SEM images of the micro-temperature sensor are shown in Figs. 5(a) and 5(b), respectively. The micro-temperature sensor composed of the Cu_2O-rich sensing part and the Cu-rich electrodes was fabricated by optimizing the laser irradiation conditions. Figures 5(c) and 5(d) show SEM images of the enlarged sensing part and the electrodes, respectively. A relatively uniform surface was obtained on the Cu_2O-rich sensing part. The thickness of the Cu_2O-rich sensing part was approximately 8 μm, which was almost the same as that of the as-coated CuO NP solution film. On the other hand, a large volume of particles were observed around the laser-scanned melted area, as shown in Fig. 5(d). It is considered that these large volumes of particles were formed in the less-heat-affected zone around the melted area, where nonirradiated CuO NPs were not melted nor removed by rinsing in the case of a single laser scan, as shown in Fig. 2(a). The thicknesses of the melted and surrounding areas were approximately 12 and 3 μm, respectively.

The resistance was 25.73 MΩ at 30°C, which was approximately 10 MΩ larger than the one estimated using the electrical resistivity of the Cu_2O-rich and Cu-rich micropatterns. This result suggests that the connecting areas between the Cu_2O-rich sensing part and the Cu-rich electrodes were reoxidized by multiple laser scans on the reduced Cu or Cu_2O. Furthermore, the volume of the multi-laser scanned area might be changed by voids that were formed during sintering and shrinking of the metal oxides. In the future, it will be important to examine in detail the composition and the density of the microstructures. The sensing part was overcoated by SiO_2 thin film by the RF magnetron sputtering method. Figure 6 shows the temperature dependence of the sensor resistance. The hysteresis of the resistance was small. The temperature coefficient of resistance was -5.5×10^{-3}/°C. This resistance property with negative value was consistent with that of semiconductor Cu_2O. The strong temperature dependence of the resistance was effective for obtaining highly sensitive temperature sensors.

4. Conclusions

A micro-temperature sensor composed of a Cu_2O-rich sensing part and Cu-rich electrodes was fabricated by femtosecond laser selective patterning using the reduction of CuO NPs.

The Cu_2O-rich and Cu-rich micropatterns were selectively formed at the laser scan speed of 1 mm/s and the pulse energy of 0.54 nJ and the laser scan speed of 15 mm/s and the pulse energy of 0.45 nJ, respectively, when the raster laser scan pitch was 5 μm. The temperature coefficient of resistance was -5.5×10^{-3}/°C. This resistance property with a negative value was consistent with that of semiconductor Cu_2O.

Acknowledgments

This study was partially supported by the Nanotechnology Platform Program (Micro-Nano Fabrication) of the Ministry of Education, Culture, Sports, Science and Technology, Japan (MEXT), and by the Cross-ministerial Strategic Innovation Promotion Program (SIP) of the New Energy and Industrial Technology Development Organization (NEDO).

References

1) Y. P. Kathuria, Surf. Coatings Technol. **116–119**, 643 (1999).
2) Y. Tang, H. T. Loh, Y. S. Wong, J. Y. H. Fuh, L. Lu, and X. Wang, J. Mater. Process. Technol. **140**, 368 (2003).
3) A. Simchi, F. Petzoldt, and H. Pohl, J. Mater. Process. Technol. **141**, 319 (2003).
4) A. Takaichi, Suyalatu, T. Nakamoto, N. Joko, N. Nomura, Y. Tsutsumi, S. Migita, H. Doi, S. Kurosu, A. Chiba, N. Wakabayashi, Y. Igarashi, and T. Hanawa, J. Mech. Behav. Biomed. Mater. **21**, 67 (2013).
5) K. A. M. Seerden, N. Reis, J. R. G. Evans, P. S. Grant, J. W. Halloran, and B. Derby, J. Am. Ceram. Soc. **84**, 2514 (2001).
6) S. B. Fuller, E. J. Wilhelm, and J. M. Jacobson, J. Microelectromech. Syst. **11**, 54 (2002).
7) X. Zhao, J. R. G. Evans, M. J. Edirisinghe, and J.-H. Song, J. Am. Ceram. Soc. **85**, 2113 (2002).
8) B. Park, D. Kim, S. Jeong, and J. Moon, Thin Solid Films **515**, 7706 (2007).
9) Y. Lee, J.-r. Choi, K. J. Lee, N. E Stott, and D. Kim, Nanotechnology **19**, 415604 (2008).
10) J. S. Kang, H. S. Kim, J. Ryu, H. T. Hahn, S. Jang, and J. W. Joung, J. Mater. Sci.: Mater. Electron. **21**, 1213 (2010).
11) M. Zenou, O. Ermak, A. Saar, and Z. Kotler, J. Phys. D **47**, 025501 (2014).
12) B. Kang, S. Han, J. Kim, S. Ko, and M. Yang, J. Phys. Chem. C **115**, 23664 (2011).
13) J. Ryu, H.-S. Kim, and H. T. Hahn, J. Electron. Mater. **40**, 42 (2011).
14) H. Lee and M. Yang, Appl. Phys. A **119**, 317 (2015).
15) D. Lee, D. Paeng, H. K. Park, and C. P. Grigoropoulo, ACS Nano, **8**, 9807 (2014).
16) D. Paeng, D. Lee, J. Yeo, J. -H. Yoo, F. I. Allen, E. Kim, H. So, H. K. Park, A. M. Minor, and C. P. Grigoropoulos, J. Phys. Chem. C **119**, 6363 (2015).
17) S. Arakane, M. Mizoshiri, and S. Hata, Jpn. J. Appl. Phys. **54**, 06FP07 (2015).
18) M. Mizoshiri, S. Arakane, J. Sakurai, and S. Hata, Appl. Phys. Express **9**, 036701 (20016).
19) S. T. Shishiyanu, T. S. Shishiyanu, and O. I. Lupan, Sens. Actuators B **113**, 468 (2006).
20) J.-W. Han and M. Meyyappan, Appl. Phys. Lett. **98**, 192102 (2011).
21) B. C. Yadav, R. Srivastava, A. K. Yadav, and T. Shukla, Int. J. Green Nanotech. **3**, 56 (2011).
22) D. O. Scanlon, B. J. Morgan, and G. W. Watson, Phys. Rev. Lett. **103**, 096405 (2009).

23) T. Mahalingam, J. S. P. Chitra, S. Rajendran, and P. J. Sebastian, Semicond. Sci. Technol. **17**, 565 (2002).
24) M. Kevin,W. L. Ong, G. H. Lee, and G. W. Ho, Nanotechnology **22**, 235701 (2011).
25) S.–B. Wang, C.–H. Hsiao, S.–J. Chang, K.–T. Lam, K.–H. Wen, S.–J. Young, S.–C. Hung, and B.–R. Huang, IEEE Sens. J., **12**, 1884 (2012).
26) X. Mathew, N. R. Mathews, and P. J. Sebastian, Sol. Energy Mater. Sol. Cells **70**, 277 (2001).
27) J. L. C. Huaman, K. Sato, S. Kurita, T. Matsumoto, and B. Jeyadevan, J. Mater. Chem. **21**, 7062 (2011).
28) J. A. Switzer, C.-J. Hung, L. –Y. Huang, F. S. Miller, Y. Zhou, E. R. Raub, M. G. Shumsky, and E. W. Bohannan, J. Mater. Res. **13**, 909 (1998).
29) T. V. Pham, M. Rao, P. Andreasson, Y. Peng, J. Wang, and K. B. Jinesh, Appl. Phy. Lett. **102**, 032101 (2013).
30) M. Y. Onimisi, Int. J. Phys. Sci. **3**, 194 (2008).

Figure Captions

Fig. 1. (Color Online) (a) Design and (b) fabrication process of Cu/Cu_2O composite micro-temperature sensor.

Fig. 2. (Color online) (a) Optical microscope and (b) SEM images of the line patterns at scan speed of 20 mm/s and pulse energy of 0.17 nJ. (c) Optical microscope and (d) SEM images of the line patterns at scan speed of 1 mm/s and pulse energy of 0.54 nJ.

Fig. 3. XRD spectra of the micropatterns (raster scan pitch: 5 μm) fabricated with various scan speeds at pulse energy of 0.54 nJ.

Fig. 4. (Color online) Intensity ratio of $I_{Cu2O(111)}/I_{CuO(111)}$ at scan pitch of (a)5 μm, (b)10 μm, and (c)15 μm. Intensity ratio of $I_{Cu(111)}/I_{Cu2O(111)}$ at scan pitch of (d)5 μm, (e)10 μm, and (f)15 μm.

Fig. 5. (Color online) (a) Optical microscope and (b) SEM images of the micro-temperature sensor. SEM images of (c) the enlarged sensing part and (d) the electrodes.

Fig. 6. (Color online) Temperature dependence of resistance of the Cu/Cu_2O composite micro-temperature sensor.

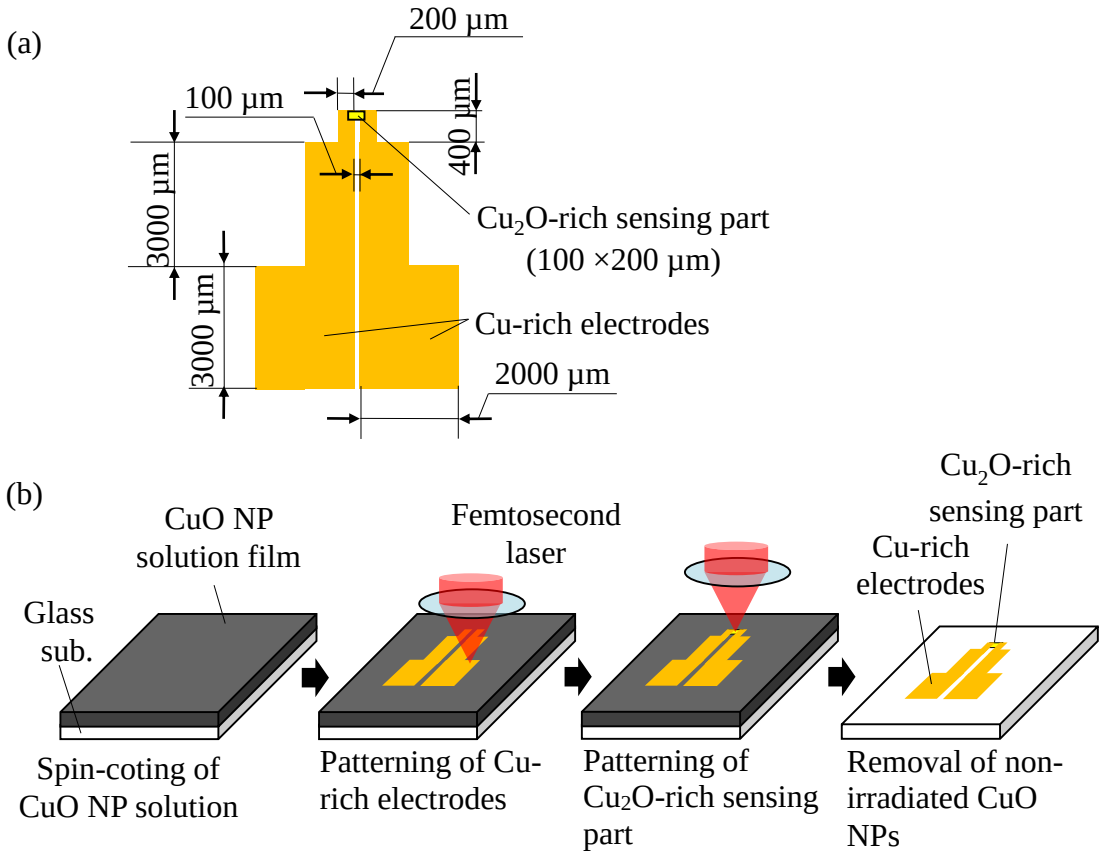

Fig.1. (Color Online) (a) Design and (b) fabrication process of Cu/Cu_2O composite micro-temperature sensor.

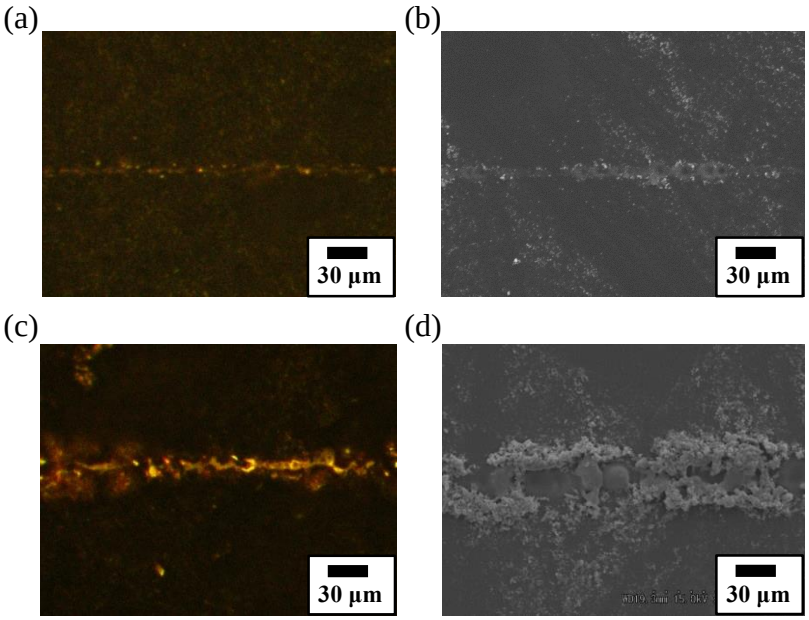

Fig. 2. (Color online) (a) Optical microscope and (b) SEM images of the line patterns at scan speed of 20 mm/s and pulse energy of 0.17 nJ. (c) Optical microscope and (d) SEM images of the line patterns at scan speed of 1 mm/s and pulse energy of 0.54 nJ.

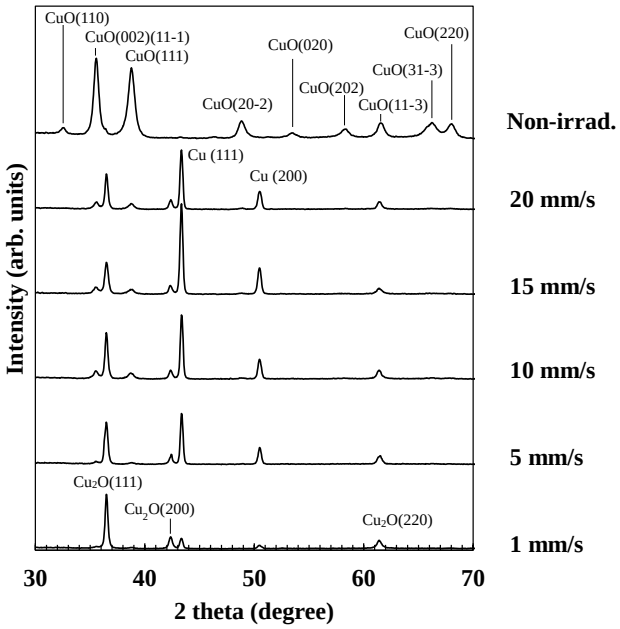

Fig. 3. XRD spectra of the micropatterns (raster scan pitch: 5 μm) fabricated with various scan speeds at pulse energy of 0.54 nJ.

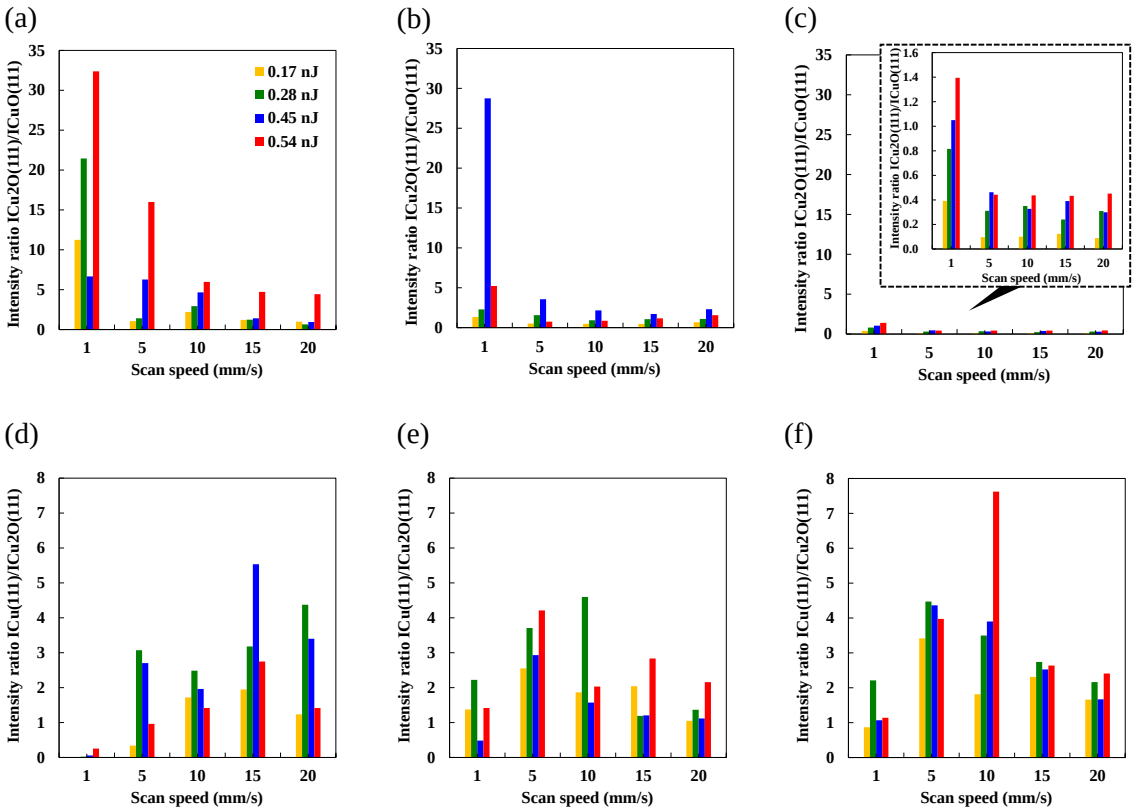

Fig. 4. (Color online) Intensity ratio of $I_{Cu2O(111)}/I_{CuO(111)}$ at scan pitch of (a)5 μm, (b)10 μm, and (c)15 μm. Intensity ratio of $I_{Cu(111)}/I_{Cu2O(111)}$ at scan pitch of (d)5 μm, (e)10 μm, and (f)15 μm.

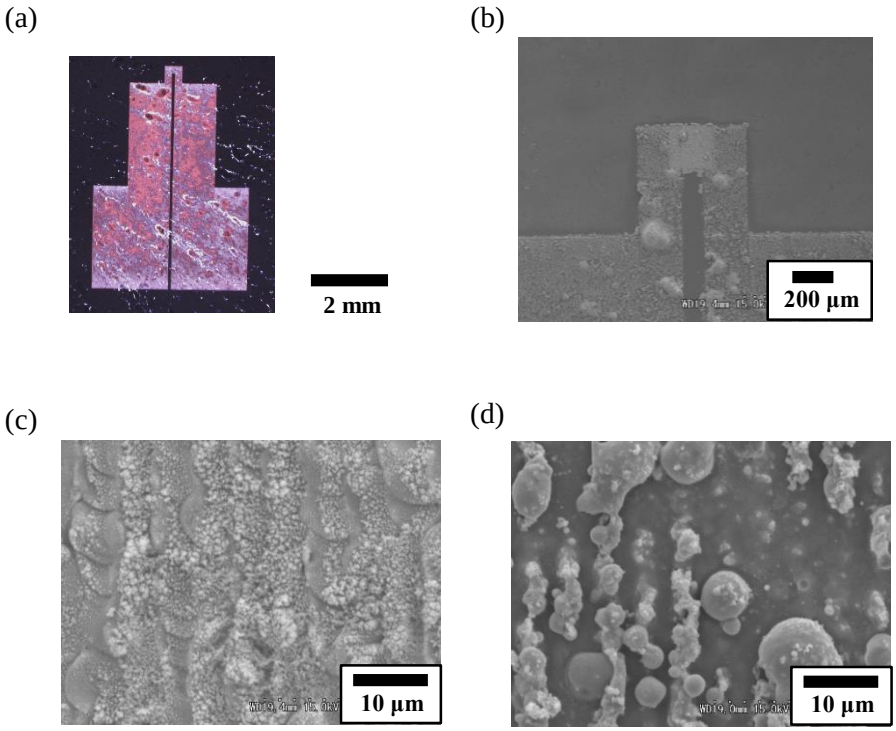

Fig. 5. (Color online) (a) Optical microscope and (b) SEM images of the micro-temperature sensor. SEM images of (c) the enlarged sensing part and (d) the electrodes.

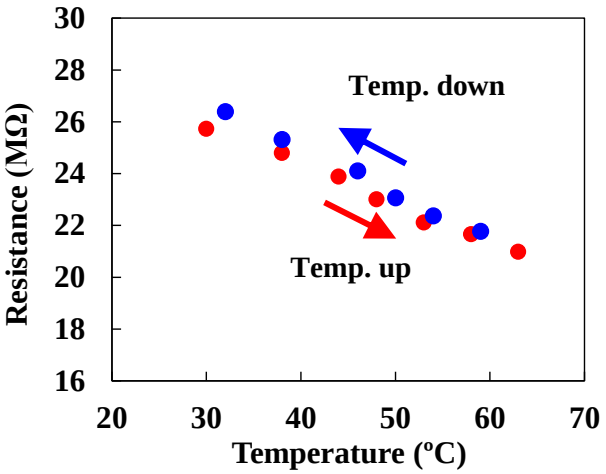

Fig. 6. (Color online) Temperature dependence of resistance of the Cu/Cu_2O composite micro-temperature sensor.